ResearchGate

See discussions, stats, and author profiles for this publication at: https://www.researchgate.net/publication/235345497

Poly(trimethylene terephthalate-block-tetramethylene oxide) Elastomer/Single-Walled Carbon Nanotubes Nanocomposites: Synthesis, Structure, and Properties

ARTICLE *in* JOURNAL OF APPLIED POLYMER SCIENCE · NOVEMBER 2012

Impact Factor: 1.77 · DOI: 10.1002/app.36961

CITATIONS
13

READS
46

1 AUTHOR:

Anna Szymczyk
Szczecin University of Technology
41 PUBLICATIONS **304** CITATIONS

SEE PROFILE

Available from: Anna Szymczyk
Retrieved on: 27 January 2016

Poly(trimethylene terephthalate-*block*-tetramethylene oxide) Elastomer/Single-Walled Carbon Nanotubes Nanocomposites: Synthesis, Structure, and Properties

Anna Szymczyk

Institute of Physics, Faculty of Mechanical Engineering and Mechatronics, West Pomeranian University of Technology, Szczecin, Piastów Av. 17, 70-310 Szczecin, Poland

Received 20 June 2011; accepted 24 January 2012
DOI 10.1002/app.36961
Published online 13 April 2012 in Wiley Online Library (wileyonlinelibrary.com).

ABSTRACT: Nanocomposites based on poly(trimethylene terephthalate)-*block*-poly(tetramethylene oxide) (PTT-PTMO)-segmented copolymer and COOH-functionalized single-walled carbon nanotubes (SWCNTs) were prepared by *in situ* polymerization method. The obtained nanocomposites were characterized by thermogravimetric analysis, scanning electron microscopy, differential scanning calorimetry (DSC), DMTA, wide-angle x-ray scattering (WAXS), small-angle X-ray scattering, and tensile testing. The nanocomposites with low SWCNTs loading (<0.5 wt %) shows uniform dispersion of CNT in polymer matrix. As the SWCNTs loading in the nanocomposites increase, the significant improvement of thermo-oxidative stability was observed. It was found that the nanocomposites have slightly higher degree of crystallinity (determined by DSC and WAXS) of poly(trimethylene terephthalate) (PTT) hard phase than neat PTT-PTMO copolymer. The melting point of PTT hard phase and glass transition temperature of poly(tetramethylene oxide)-rich phase were not affected by the presence of CNTs in polymer matrix. The SWCNTs played a role as nucleating agent in PTT-PTMO matrix, which led to increase in the crystallization rate. Tensile tests showed that the tensile strength of the nanocomposites with 0.05–0.3 wt % loading of SWCNTs have improved tensile strength in comparison to the neat PTT-PTMO copolymer without reduction elongation at break. © 2012 Wiley Periodicals, Inc. J Appl Polym Sci 126: 796–807, 2012

Key words: polymer nanocomposites; polyester thermoplastic elastomer; carbon nanotubes

INTRODUCTION

Polymeric nanocomposites or polymer nanostructure materials have been widely investigated due to its outstanding properties. The incorporation of nanometer scale reinforcement in many polymer systems may dramatically improve selected properties of the related polymer. Besides, nanometer-sized filler materials with their inherently large surface area to volume ratios are particularly very interesting as they facilitate increases in the efficiency of a given property. A desired property or level of property enhancement can be achieved at very low loading of nanofillers into polymer matrix. Dependent on the type of used nanofiller [carbon nanotubes (CNTs), graphene, and nanoclays], the nanocomposites exhibit superior properties such mechanical and electrical properties, reduced permeability, and improved flame retardancy.[1–4] Among nanofillers, CNTs have attracted interest as reinforcing fillers because their extraordinary mechanical properties (Young's modulus: 1 TPa, tensile strength: 100–150 GPa).[5] In addition to their exceptionally high electrical conductivity, they are also regarded as the ultimate fillers for creating electrically conductive polymer nanocomposites. CNTs as reinforcements in many polymers matrixes (thermoplastics, thermosets, or elastomers) have already been used.[2,5–7] The number one challenge to incorporate CNTs as fillers for polymers is dispersion. It is known that to transfer the outstanding mechanical properties of CNTs to the composite material one essential and difficult step involves the fine dispersion of the nanotubes within the polymer matrix. Van der Waals forces, which cause the CNTs to clump together and form aggregates, must be overcome. Earlier studies on polyester/CNTs nanocomposites[8–12] have shown that *in situ* polymerization method is very effective. The obtained poly(ethylene terephthalate) (PET)-,[8,9] poly(trimethylene terephthalate) (PTT)-,[10] and poly (butylene terephthalate) (PBT)[11,12]-based nanocomposites are characterized by uniform dispersion of CNTs in polymer matrix, enhanced mechanical and electrical properties, and can be processed by injection molding. Specific influence of CNTs on the mechanical properties can be expected if the nanoheterophase-structured polyester block copolymers are used as matrix.

Correspondence to: A. Szymczyk (aszymczyk@zut.edu.pl).
Contract grant sponsor: Polish National Science Centre; contract grant number: 2183/B/T02/2011/40.

© 2012 Wiley Periodicals, Inc.

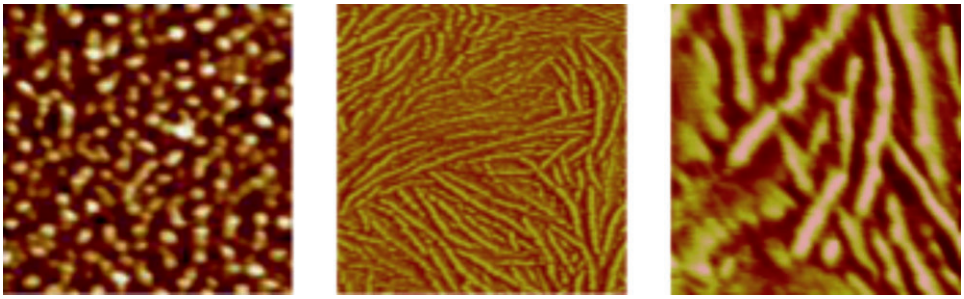

Figure 1 AFM phase images of: (a) PBT-*block*-PTMO (50 : 50 wt %) (microtome cross-section) and (b) PTT-*block*-PTMO (50 : 50 wt %) (film-cast from solution). The scan boxes are 200 × 200 (a and c) nm and 500 × 500 nm (b) (unpublished own results). [Color figure can be viewed in the online issue, which is available at wileyonlinelibrary.com.]

Commercially important thermoplastic polyester elastomers (TPE-E) possess a blocky chain structure consisting of a high melting polyester block and low glass transition polyether block.[13] Since the early work of Cella,[14] it has been established that segmented polyester block copolymers generally microphase separate into high melting crystalline "hard" domains and relatively low glass transition (T_g) "soft" domains, on cooling from the melt or precipitation from solution. The degree to which these copolymers phase separate significantly affects many of the physical properties of these materials. On atomic force microscopy (AFM) phase images in Figure 1, we can observe the nanoseparated structure of segmented polyester block copolymers, based on PBT or PTT as "rigid" blocks and poly(tetramethylene oxide) (PTMO) as "soft" blocks. The hard phase appears lighter than the soft phase in these images. As can be seen, the hard blocks from domains of the order of several nanometers that serves as reinforcements and as physical crosslinks to connect the elastomeric soft blocks.

In this work, the possibility of obtaining nanocomposite material based on thermoplastic polyester elastomer and COOH-functionalized SWCNTs was studied. Nanocomposites with low loading of SWCNTs were prepared by *in situ* polymerization method. Segmented block copolymer with crystallizable PTT rigid segments and PTMO as flexible segments was chosen as polymer matrix. The PTT and PTMO segments may segregate into separate phases in the solid state as other segmented copolymers do due to the thermodynamic immiscibility of the rigid and flexible segments. As can be seen on Figure 1(b,c), the morphology in this copolymer consists of semicrystalline PTT domains (very thin ribbonlike crystallites) dispersed in the soft matrix (dark region) of amorphous, noncrystallizable PTMO.[13] The nanometric structure of segregated rigid and soft segments is mainly responsible for the mechanical properties of these polymers.[15,16] These kinds of semicrystalline thermoplastics elastomers can be seen as nanocomposites by themselves, as they are composed of an amorphous phase (PTMO) and crystalline lamellae (PTT). As can be seen from Figure 1(b), the hard segment crystalline lamellae up to 11 nm in width, but several hundreds of nanometers in length can play the same role as nanofillers.[17] The crystallization of the polyester "rigid-segment" sequences is an important factor governing the formation of physical crosslinks and subsequent mechanical properties in these materials. The addition of a low quantity of CNTs can change the macroscopic properties (for instance tensile properties) of semicrystalline TPE-E, when a synergy between the crystalline lamellae of polymer and the CNTs is created. A synergy between the CNTs and the crystalline lamellae of the polymer is, however, not sufficient to obtain improved mechanical properties, because a good dispersion of the CNTs has to be ensured. In nanocomposites can be also present some regions with given orientations of CNTs and the lamellae (hybrid shish-kebab superstructures) which probably can also play role in improvement of mechanical properties.[7,12]

Effect of the CNTs presence in homopolymer PTT matrix on nonisothermal crystallization behavior was studied in previous author work[10,18] and other researches.[19–21] It was found that crystallization of PTT-based nanocomposites is strongly dependent on the type of used CNTs and their preparation method. For Example, the PTT/SWCNTs composites[18] present a higher overall crystallization rate than that of the neat PTT due to the nucleation effect of the SWCNTs. While the introduced short and thin COOH-functionalized multi-walled carbon nanotubes (MWCNTs) into PTT matrix were not effective nucleating agent caused the increased of the degree of supercooling.[10] Here, the effect of the presence of COOH-functionalized SWCNTs in PTT-PTMO matrix on phase structure and mechanical properties were investigated.

EXPERIMENTAL

Materials

For the preparation of nanocomposites, the following materials were used: dimethyl terephthalate (DMT,

Sigma-Aldrich); 1,3-propanediol (PDO, Shell Chemicals); poly(oxytetramethylene glycol) with molecular weight of 1000 g mol^{-1} (PTMG, Terathane 1000 DuPont); antioxidant *N*,*N*′-diphenyl-*p*-phenylendiamine (DPPD, Bayer); anhydrous *N*-methyl-2-pyrrolidone (NMP, Sigma-Aldrich). The PDO was distilled before using. As catalyst the tetrabutyl orthotitanate ($Ti(OBu)_4$, Fluka) was used as receive. As catalyst the $Ti(OBu)_4$ (Fluka) was used as receive. The COOH-functionalized single-walled carbon nanotubes (SWCNTs, purity >95%) with diameter 1–2 nm, length < 30 μm, and COOH functionalization 1–4 wt % were purchased from Array.

Preparation of nanocomposites

The PTT-PTMO/SWCNTs nanocomposites were prepared by a two-step melt polycondensation method as follows. The DMT (110.2 g and 0.57 mol) and PDO (67.7 g and 0.89 mol) were charged into well dried 1 dm^3 steel reactor (Autoclave Engineers PA) equipped with condenser, a stirrer, and gas inlet. The SWCNTs were dispersed in 300 mL of NMP by using ultrahigh speed stirring and ultrasonication. Total time of dispersing was 30 min. Then the dispersion was introduced into reaction mixture containing PDO and melted DMT. The first step of polycondensation, the transesterification reaction, was carried out under a constant flow of nitrogen at 160°C in the presence of catalyst ($Ti(OBu)_4$, 0.2 wt % in relation to DMT). During the reaction, DMT was transesterified with PDO and methanol being released in the reaction was distilled out of the reaction mixture at atmospheric pressure. After 1.5 h to the reaction mixture, which comprises mostly bis-(3-hydroxypropyl) terephthalate, the PTMG (122.1 g, 0.12 mol), DPPD (0.5 wt % of total comonomers mass) and second portion of catalyst (0.15 wt %) were introduced to the reactor. Then the reaction temperature was increased slowly to 220°C, and the pressure was reduced slowly. When the NMP was distilled off, the reaction temperature was increased to 245°C and pressure reduced below 20 Pa for the second step of the polycondensation reaction. The stirring torque change was monitored to estimate the melt viscosity of the product. All syntheses of the nanocomposites were finished when melt reach the same value of viscosity at 245°C. The molten composite was extruded from reactor into water cooling bath, and then granulated and dried before processing. At the same conditions as nanocomposites, the neat PTT-PTMO copolymer was synthesized as reference. Nanocomposites and the neat PTT-PTMO block copolymer with the content of 40 wt % of PTT rigid segments and 60 wt % of PTMO soft segments were obtained. The obtained PTT-PTMO nanocomposite samples were coded as PEE/x, where x denotes the weight fraction of SWCNTs.

Sample preparation

Samples for DMTA, wide-angle x-ray scattering (WAXS), small-angle X-ray scattering (SAXS), and tensile testing were prepared by injection molding at a pressure of around 50 MPa. The temperatures were ~ 10°C higher than the melting point of the polymers determined by differential scanning calorimetry (DSC), whereas the mold temperature was kept at 40°C.

Measurements

Limiting viscosity number [η] of the neat PTT-PTMO block copolymer and nanocomposites was measured in a mixture of phenol/1,1,2,2-tetrachloroethane (60/40 wt/wt) at temperature of 30°C, using an Ubbelohde viscometer with capillary 1c (K = 0.03294). The concentration of the polymer in the solution was 0.5 g dL^{-1}. The melt flow rate (MFR) was measured on a melt indexer (CEAST, Italy) according to ISO 1133 specification at temperature 195°C.

DSC was carried out on the TA Q 100 instrument (TA Instruments), at a heating rate of 10°C min^{-1} from −100 to 250°C. Temperature and heat transition were calibrated with indium standard. Each DSC testing cycle consisted of heating, cooling, and repeating the scans. The crystallization and melting temperatures (T_c and T_m) were determined from the maximum the exothermic and endothermic peaks, respectively and the glass transition temperatures (T_{g1} and T_{g2}) were taken as the midpoints of the heat capacity change ($\Delta C_p/2$). The degree of crystallinity (x_c) of hard segment phase in the copolymer was calculated as the ratio: $x_c = (\Delta H_m/\Delta H_m^0)$ 100%; where: ΔH_m is the heat fusion of sample estimated from second heating scan, and $\Delta H_m{}^o$ is the heat of fusion fully crystalline PTT (ΔH_m^0 = 146 J mol^{-1}).[22]

The dynamic mechanical thermal (DMTA) measurements were preformed with a Polymer Laboratories MK II apparatus working in a bending mode. A frequency of 1 Hz and a heating rate of 3°C min^{-1} from −100 to 200°C were used.

The tensile properties were determined according to DIN 53544, on compression-molded dumbbells. The measurements were conducted at a constant testing rate of 50 mm min^{-1} and room temperature. Each value represents an average of seven measurements.

The morphology of the composites was observed with a scanning electron microscope (SEM, JEOL JSM-6100) at an accelerating voltage of 20 kV. Before analysis, the samples were cryofractured in liquid nitrogen, and then coated with a thin homogenous gold layer by ion-sputtering gold.

The thermogravimetric analysis (TGA) of nanocomposites was obtained using an instrument under a SETARAM TGA 92-16 apparatus under dynamic atmosphere of argon and air (the flow rate was 20 cm^3 min^{-1}), at hating rate of 10°C min^{-1}.

WAXS experiments were carried out using a URD-6 Seifert diffractometer operated at 40 kV and 30 mA. Ni-filtered CuK_α radiation with wavelength of $\lambda = 1.54$ Å was applied. Diffraction patterns were recorded with a 0.1° step in the 2θ range from 4° to 60° at room temperature. The WAXS curves were analyzed and degree of crystallinity was calculated with the WAXSFit computer program.[23] The degree of crystallinity (x_c) was calculated as the ratio of the total area under the resolved crystalline peaks to the total area under the unresolved X-ray scattering curve.

SAXS measurements were carried out using a modified Kratky compact camera (MBraun). The primary X-ray beam of 1.542 Å wavelengths was produced by anode generator (40 kV and 30 mA) and Ni-filtering. The measurements where preformed in the s—range from 1.1×10^{-3} Å^{-1} to 5.4×10^{-2} Å^{-1}; where $s = (4\pi/\lambda)\sin\theta$—is the scattering vector, and 2θ is the scattering angle. Exposure times were typically 1800 s for individual measure. The detailed parameters of lamellar structures, such as long period (L), crystal thickness (l_c), amorphous layer thickness (l_a), transition layer thickness (E) were determined from the one-dimensional correlation function $\gamma(r)$[24–27] calculated from the corrected SAXS data by using computer program SAXSDAT.[28] The correlation function is the Fourier transform of the Lorentz-corrected SAXS data as given in eq. (1):

$$\gamma(r) = \frac{\int_0^\infty I(s)s^2\cos(2\pi sr)ds}{\int_0^\infty I(s)s^2ds} \quad (1)$$

where $I(s)$ is scattering intensity, and r is the distance in real space. The correlation function was normalized to the unity in the origin by dividing liner correlation function (2)[26,27] by invariant Q (3):

$$K(r) = \int_0^\infty I(s)s^2\cos(2\pi sr)ds \quad (2)$$

$$Q = \int_0^\infty I(s)s^2ds \quad (3)$$

The in variant Q is the total scattering power of the system, which is independent of the size and shape of the scattering entitles. For a two-phase lamellar structure, the invariant can be directly proportional to the volume fraction of the crystallites, ϕ_c, by:

$$Q = \phi_c(1 - \phi_c)\Delta\rho_e \quad (4)$$

where $\Delta\rho_e$ denotes the electron intensity contrast between crystalline and amorphous layers. Because SAXS data are collected in a limited angle range, the SAXS data were extrapolated to both high and low s values before Fourier transformation. The long period (L) was estimated from the position of the first maximum of $\gamma(r)$ [see later Fig. 7(b)], and the thickness of the crystalline and amorphous layers in the stacks was calculated as follows:

$$l_c = \phi_c L,\ l_a = L(1 - \phi_c) \quad (5)$$

The transition layer (E) between the amorphous and crystalline regions was calculated from

$$E = 3(1 - Q/Q_i)R \quad (6)$$

where $R = L\phi_c(1 - \phi_c)$ is the position of the first intercept of the correlation function with the r-axis.[29]

RESULTS AND DISCUSSION

PTT-PTMO block copolymer nanocomposites containing from 0.05 to 0.5 wt % of COOH-functionalized SWCNTs were prepared by using *in situ* polymerization method. The advatage of this method is that it can be easily adopted to manufacture of these kind of nanocomposites in industrial scale. In prevoius studies[7,8,30] it has been shown that the crucial issue in obtaining of uniform distribution of CNTs in polymer matrix is the dispergantion of CNTs in liquid substrate or solvent additionally introduced into reaction mixture. Recently, NMP was find as a good solvent for graphene and CNTs dispersion.[31,32] Here, COOH-functionalized SWCNTs were sonicated and mechanicallly stirred in NMP to break existed agglomerates. All syntheses of the nanocomposites were finished, when melt reach the same value of viscosity at 245°C. At the same conditions as nanocomposites the neat PTT-PTMO block copolymer was synthesized as reference. The highest content of COOH-functionalized SWCNTs achieved in the prepared nanocomposites was 0.5 wt %. The introduction of higher content of CNTs was not possible because, the melt does not flow. The content of PTT rigid segments was 40 wt % and the content of PTMO soft segments was 60 wt %. The morphology in this copolymer consisted of semicrystalline PTT domains dispersed in the soft matrix of amorphous, noncrystallizable PTMO.[15,16] The average molecular weight of the copolymer was $\sim$ 41,000 g mol^{-1}.[15] In Table I, basic physical properties of obtained PTT-PTMO/SWCNTs nanocomposites are presented. As the content of CNTs increases, the nanocomposites have lower values of the limiting viscosity number than neat PTT-PTMO block copolymer which can indicate that they have lower molecular weights. The values of the MFR of nanocomposites are lower in comparison to the neat PTT-PTMO block copolymer. The lower values of MFR suggest that

TABLE I
Characteristics of PTT-PTMO/SWCNTs Nanocomposites

Sample	w_{CNT} (wt %)	[η] (dL g^{-1})	MFR (g 10 min^{-1})	$T_{10\%}$ [a] (°C)	$T_{10\%}$ [b] (°C)
PEE/0	0	1.73	6.1	334	379
PEE/0.05	0.05	1.70	4.9	341	382
PEE/0.1	0.1	1.72	6.0	352	383
PEE/0.2	0.2	1.70	5.7	360	383
PEE/0.3	0.3	1.69	4.6	347	383
PEE/0.5	0.5	1.66	3.8	365	384

w_{CNT}, weight content of SWCNTs; MFR, melt flow rate at 195°C; $T_{10\%}$, temperature of 10 weight % loss in air[a] and in argon[b].

nanocomposites have higher melt viscosity due to the presence of and CNT–polymer and CNT–CNT interactions.

SEM morphology of PTT-PTMO/SWCNTs nanocomposites

The morphologies of the PTT-PTMO/SCWNTs nanocomposites are shown in Figure 2(a–f). From the SEM images of the fractured surface of PTT-PTMO/SCWNTs nanocomposites, it can be seen that SWCNTs are randomly dispersed in PTT-PTMO matrix. Individual nanotubes, some entanglements or bundles of CNTs, apparently pulled out from the matrix during fracturing can be observed. Only a very few agglomerates [as on Fig. 2(f)] are observed for samples with the highest concentration of CNTs in PTT-PTMO matrix. No apparent damage or breakdown of the nanotubes was observed. The carboxylic groups seem to stabilize the SWCNTs-dispersion by interaction with PTT-PTMO matrix. This can be attributed to the increase of polarity of the SWCNTs by the presence of carboxylic groups and their possible reaction with the PTT-PTMO copolymer, forming covalent bonding and also by the presence of hydrogen bonding between CNTs and the ester groups of the PTT-PTMO matrix. The remaining polymer layer coating CNTs [Fig. 2(a,c)] indicates a very strong matrix adhesion. It is seen also that the both ends of SWCNTs are tightly embedded in PTT-PTMO matrix indicating the existence of strong interfacial adhesion between the SWCNTs and matrix. Usually, in oxidized CNTs, the COOH groups dominated at the ends of CNTs.[33] Therefore, the ends of used SWCNTs can posses more COOH groups and the interaction between their ends and matrix can be much stronger than between their side-walls and matrix. Hence, the good interfacial adhesion between SWCNTs and the PTT-PTMO matrix may be also responsible for enhancement of the mechanical properties of PTT-PTMO nanocomposites with a very small quantity of the COOH-functionalized SWCNTs. Recent investigations of nanocomposites based on polyester such as PEN,[34,35] PET,[36] and PLA[37] have showed that modification of the CNTs surface by carboxylic groups improved interfacial adhesion between CNTs and polymer matrix mainly due to the possible interaction of hydrogen bonding between the COOH groups of CNTs and the ester groups in polymer matrix. It was also established that functional groups in the carboxylic MWCNTs showed active enough for participating the polycondensation of L-lactic acid[37] and as a result of this reaction, the PLA-*grafted*-MCWNTs are formed. *In situ* polymerization method enables covalent bonding between functionalized nanotubes and the polymer matrix using various condensation reactions. For example, Zhu et al.[38] prepared epoxy nanocomposites by end-cap carboxylated SWCNTs and an esterification reaction. The functionalized CNTs were observed to be highly dispersed and well integrated in the epoxy matrix. The obtained epoxy nanocomposite containing 1 wt % of SWCNTs shows enhancement of mechanical properties, i.e., a 30% increase in modulus and 18% increase in tensile strength.

Thermal stability

PTT-PTMO copolymer as other PTMO-based poly (ether-esters) is sensitive to oxidative degradation due to the ether soft segment. The mechanism of the thermo-oxidative degradation of these copolymers involves a radical chain process with formation of hydroperoxides at the carbon adjacent o the ether oxygen.[39,40] The hydroperoxides undergo further reactions leading to new esters and oxidized products formed after chain scission, such as acids, formates, and alcohols.[39] The effect of the presence of COOH-functionalized SWNTs in PTT-PTMO matrix on thermal and oxidative stability of composites was studied by TGA. The mass loss (TG) and the DTG (derivative TG) curves under oxidative (air) and inert (argon) atmosphere of nanocomposites are shown on Figure 3(a–d). In Table I, temperatures corresponding to the 10 % weight loss ($T_{10\%}$) are presented. In argon, PTT-PTMO copolymer decomposes in a single step beginning at $\sim$ 310°C. For nanocomposites, the temperature at maximum of weight loss rate [peak on DTG curve, Fig. 3(d)] and the $T_{10\%}$ are slightly shifted (about 3–5°C) to higher temperatures suggesting higher thermal stability than neat PTT-PTMO copolymer. The improved thermal stability can be attributed to the effect of higher thermal conductivity in the polymer/CNTs nanocomposites that facilitates heat dissipation within composite. In air, PTT-PTMO block copolymer decompose in three weight-loss steps in the temperature ranges 250–346, 346–450, and 450–560°C [Fig. 3(a,b)]. The first and second steps are attributed

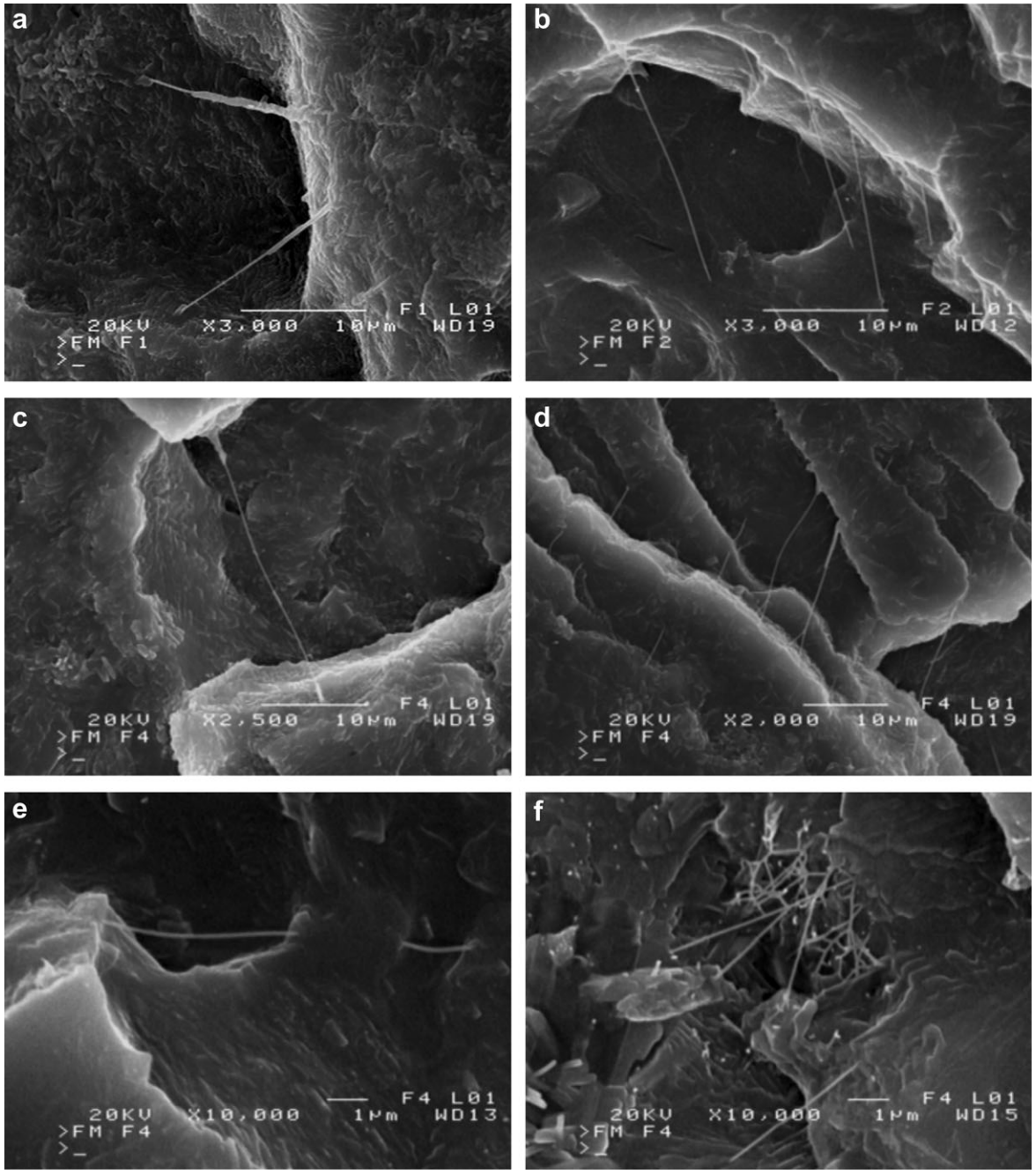

Figure 2 Representative SEM images of the PTT-PTMO/SWCNTs nanocomposites containing 0.2 (a and b), 0.3 (c and d), and 0.5 (e and f) wt % of COOH-functionalized SWCNTs.

to the decomposition of flexible (PTMO) and rigid (PTT) segments. The third step is attributed to the decomposition of residue. Addition of SWCNTs has improved thermo-oxidative stability of PTT-PTMO copolymer. The first stage of decomposition is strongly influenced by the presence of SWCNTs, the values of $T_{10\%}$ and the temperature at the maximum decomposition rate of stage is shifted ($\Delta T_{10\%} = 7$–$31^{\circ}C$) to higher temperatures. These effect can be a result of high electron affinity of CNTs similar to those of fullerenes (C_{60} and C_{70});[41] therefore, they are capable of acting as radical scavengers in free radical chain reactions, including polymerization and the thermo-oxidative degradation of polymers.[42]

Phase behavior of the PTT-PTMO/SWCNTs nanocomposites

Effect of the presence of COOH-functionalized SWCNTs on the phase structure of the PTT-PTMO nanocomposites was studied by using DSC and DMTA analyses. The DSC curves of the PTT–

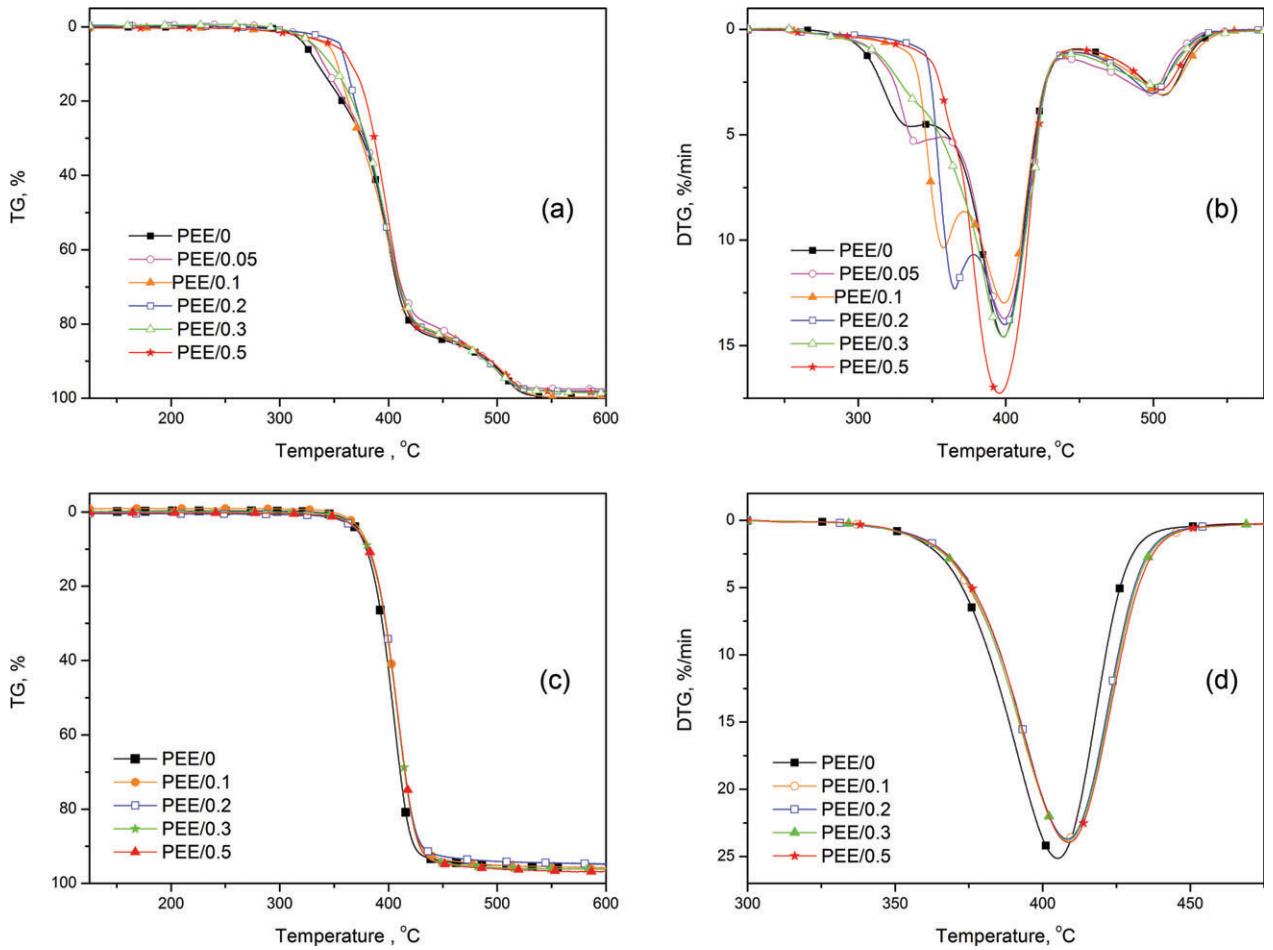

Figure 3 TG (a and c) and DTG (b and d) curves for PTT-PTMO/SWCNTs nanocomposites under air (a and b) and argon (c and d) atmosphere at heating rate 10°C min^{-1}. [Color figure can be viewed in the online issue, which is available at wileyonlinelibrary.com.]

PTMO/SWCNTs nanocomposites are shown in Figure 4, and the results are summarized in Table II. The glass transition temperatures, corresponding to the mixed amorphous flexible segments and PTT rigid ones (T_{g1}) as well as the amorphous rigid segments (T_{g2}), respectively, and the melting point derived from rigid PTT segments (T_m) were observed in DSC curves of the neat PTT-PTMO block copolymer and nanocomposites. The presence of SWCNTs in PTT-PTMO matrix does not affect on the glass transition temperatures T_{g1} and T_{g2}, and melting point [Fig. 4(a), Table II] of the PTT-PTMO matrix. However, the crystallization temperature [Fig. 4(b)] of the nanocomposites significantly increased with the concentration of CNTs, indicating the efficiency of them as strong nucleating agent for crystallization of PTT rigid segments, resulting in the enhancement of the crystallization of PTT-PTMO nanocomposites in the presence of COOH-functionalized SWNTs. The crystallinity of the nanocomposites was found to be slightly higher than of neat PTT-PTMO block copolymer, but differences between the levels of crystallinity of the samples are lower than 3%. For most nanocomposites,[10,12,35,43–48] the addition of CNTs generally results in an enhanced nucleation at low CNTs content. The few exceptions to this include poly(ethylene oxide) (PEO)/MWCNTs[49] and PEO/SWCNTs[50] nanocomposites, in which antinucleation effects (reduced crystallization rate) of CNTs have been noted. Such enhancement is usually noted for low CNTs contents, while higher contents are reported to cause reduce crystal growth rate. Müller et al.[51] have shown that in nanocomposites, a competition between supernucleation and confinement occurs. At low contents, the nucleation effect dominates. The confinement increases as the CNTs increases. In consequence of confinement, the reduction of both crystallization and melting temperatures, a strong reduction of the crystallinity degree, an increase in the supercooling needed for isothermal crystallization, and a depression of the overall crystallization rate were observed.[51] It was also reported that during CNTs-induced crystallization the nanohybrid shish-kebab structures can be formed, where the SWNT act as the shish and the epitaxial grown

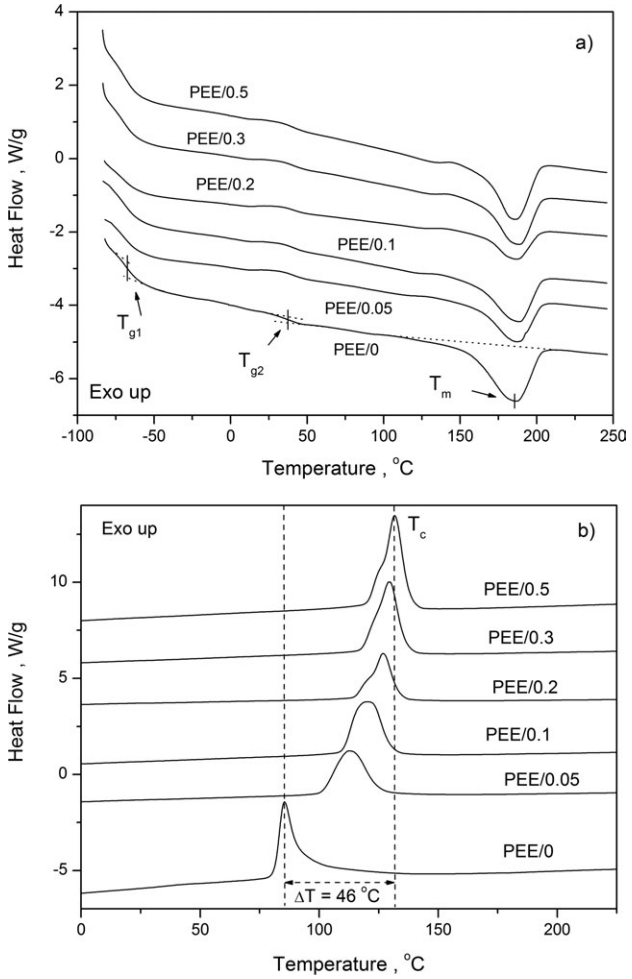

Figure 4 The DSC curves of the heating (a) and cooling (b) runs for PTT-PTMO/SWCNTs nanocomposites.

polymer crystals perpendicular to the SWCNT are the kebabs.[12,52,53] The presence of these structures has effect on mechanical properties of nanocomposites. Earlier study of nanocomposites based on SWCNTs and PBT-PTMO block copolymer[7] have shown that the CNTs can act as an anchor for the crystalline blocks in nanocomposites, sharing the applied stress with PBT crystals and making the rigid block destruction more efficient. These nanocomposites in relation to the neat copolymer have shown increase of the Young's modulus and the yield strength as well as increase of the rigidity of nanocomposites, which in consequence decrease the elongation to break. Figure 5 shows the results of DMTA analysis: a storage modulus (E'), loss modulus (E''), and loss tangent (tan δ) for nanocomposites and neat PTT-PTMO block copolymer as a function of temperature. The glass transition temperature of the PTMO-rich soft phase was identified by a drop in storage modulus (E') and β_1-relaxation peak in the E'' and tan δ curves. The melting of the rigid PTT segments caused a second strong change in the E' and E'' curves. As can be seen in Figure 5(b), the PTT-PTMO copolymer had a glass transition temperature ($T_{\beta 1}$) of ~ -48°C (determined at maximum of β_1-relaxation peak). The $T_{\beta 1}$ of nanocomposites is not influenced by the presence of CNTs, except

TABLE II
DSC Data for PTT-PTMO/SWCNTs Nanocomposites

Samples	T_{g1} (°C)	Δc_{p1} (J g°C^{-1})	T_{g2} (°C)	T_m (°C)	ΔH_m (J g^{-1})	T_c (°C)	ΔH_c (J g^{-1})	x_c (%)
PEE/0	−69	0.24	40	186	22.3	86	21.4	15.3
PEE/0.05	−69	0.25	41	187	24.1	112	23.1	16.5
PEE/0.1	−69	0.24	42	188	26.4	120	24.1	18.1
PEE/0.2	−68	0.24	42	186	24.0	127	23.9	16.4
PEE/0.3	−69	0.24	41	188	25.9	129	24.1	17.8
PEE/0.5	−69	0.25	41	186	25.5	132	23.3	17.5

T_{g1}, glass transition temperature of soft phase; Δc_{p1}, heat capacity of flexible segments; T_{g2}, glass transition temperature of amorphous polyester phase; T_m, ΔH_m, temperature and enthalpy of melting of polymer respectively; T_c, ΔH_c, temperature and enthalpy of crystallization of polymer respectively; x_c, degree of crystallinity.

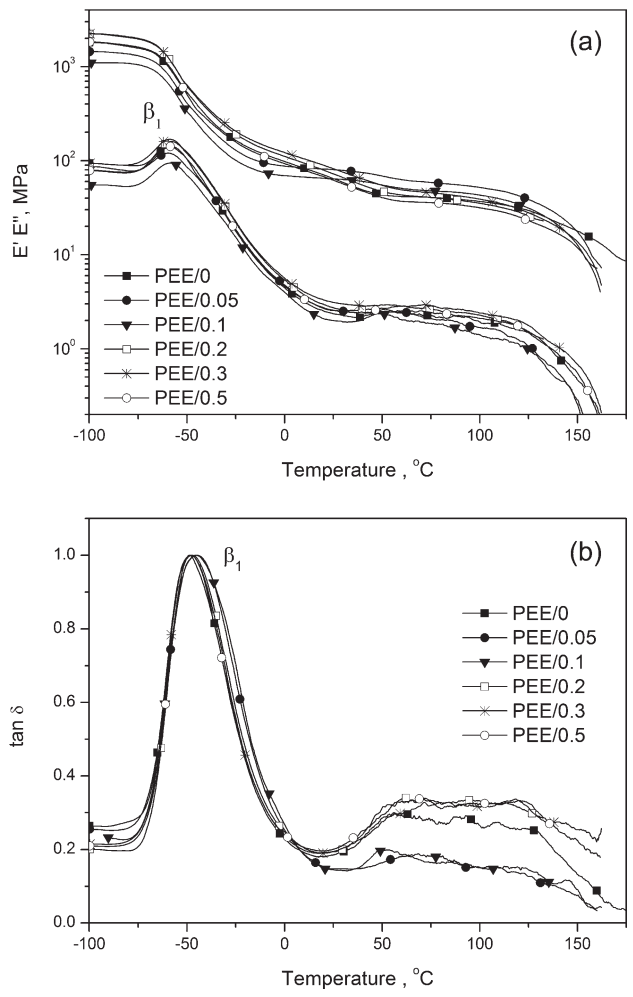

Figure 5 The storage and loss modulus (a) and normalized loss tangent (b) as a function of temperature for PTT-PTMO/SWCNTs nanocomposites.

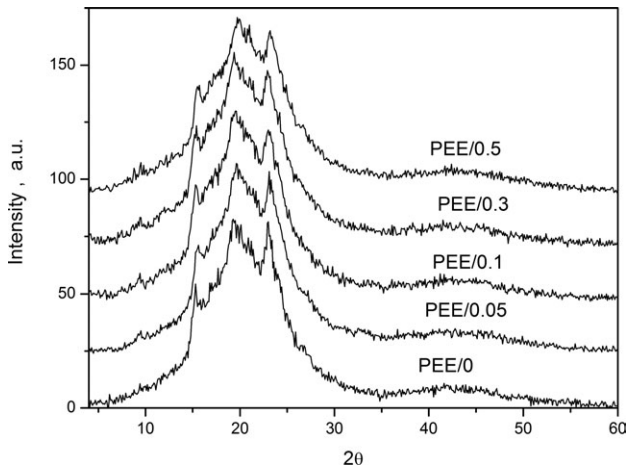

Figure 6 WAXS scans of the PTT-PTMO/SWCNTs nanocomposites.

samples containing 0.05 and 0.1 wt % of CNTs. The slightly broadening of tan δ peak for the samples PEE/0.05 and PEE/0.1 can correspond to increase in the amount of material participating in the transition. This change is probably either due to increase in the amount of the PTT noncrystallized sequences in PTMO-rich soft amorphous phase or a increasing in the mobility of the soft phase. The values of the modus in rubbery plateau and the nanocomposites containing from 0.05 to 0.3 wt % of SWNTs shows higher values of the modus in rubbery plateau than neat PTT-PTMO copolymer which can indicate higher crystallinity of hard phase. The softening temperatures had comparable values as the melting temperatures obtained with DSC analysis.

DSC and DMTA analyses were supported by WAXS and SAXS analyses. Figures 6 and 7(a) presents the WAXD and SAXS patterns obtained for PTT-PTMO nanocomposites prepared by injection molding. All of the WAXS diffractograms exhibited major characteristic crystalline peaks at scattering angles 2θ of 15.3 ± 0.1, 16.8 ± 0.1, 19.4 ± 0.1, 21.8 ± 0.1, 23.6 ± 0.1, 24.6 ± 0.1, and 27.3 ± 0.1, corresponding to the reflection planes of (010), (0$\bar{1}$2), (012), (10$\bar{2}$), (102), (1$\bar{1}$3), (10$\bar{4}$), respectively. According to published work on crystallographic studies of PTT,[54–56] the crystalline structure of these samples deduced from the diffractograms shown in Figure 6 can be designated as a triclinic unit cell parameters a = 4.62 Å, b = 6.27 Å, and c = 18.64 Å and α = 98°, β = 90°, and γ = 111°,[56] in which one chemical repeating unit of PTT is an antichiral packed along the c-axis. The calculated degree of crystallinity values (x_c) for nanocomposites (Table III) are slightly higher in comparison to the neat PTT-PTMO copolymer, as was also confirmed by DSC results. The values obtained for the different nanocomposites are in very good agreement with those derived from DSC

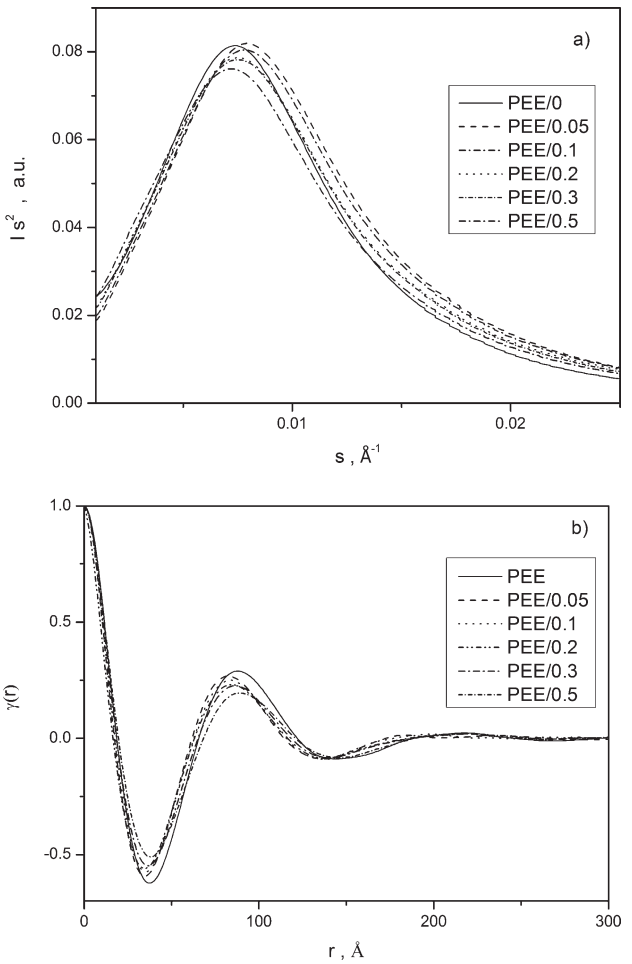

Figure 7 The Lorenz corrected SAXS profiles (a) and normalized correlation functions (b) for PTT-PTMO/SWCNTs nanocomposites.

results. On the basis of these results, we can indicate that SWCNTs in these system act as very active heterogeneous nucleation sites for PTT crystallization (strong decrease of supercooling, see Table II), but formation of CNTs network causes restriction on polymer chain diffusion and crystal grown can be limited. Hence, only slightly increase of crystallinity is observed.

TABLE III
WAXS and SAXS Data for PTT-PTMO/SWCNTs Nanocomposites

	PEE/0	PEE/0.05	PEE/0.1	PEE/0.2	PEE/0.3	PEE/0.5
x_c^w (%)	15.6	17.2	17.6	–	18.6	18.4
L (Å)	87.05	82.47	83.31	88.64	89.56	96.83
l_c (Å)	28.01	26.54	26.31	26.95	27.35	28.35
l_a (Å)	59.04	55.93	57.00	61.69	62.21	68.48
E (Å)	13.31	10.28	10.31	10.64	10.84	11.04

x_c^w, degree of crystallinity from WAXS; L, long period, l_c, crystal thickness; l_a, amorphous layer thickness; E, transition layer thickness.

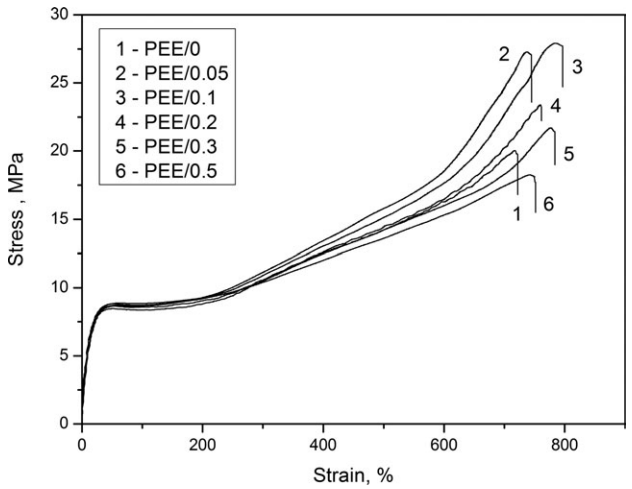

Figure 8 Stress–strain curves of PTT-PTMO/SWCNTs nanocomposites.

SAXS scattering patterns for nanocomposites after Lorentz correction are shown in Figure 7(a). Changes in lamellar nanostructure after introduction CNTs into PTT-PTMO matrix were estimated from the correlation functions (see Refs. [26] and [27]) presented on Figure 7(b). The values of the long period (L), crystal thickness (l_c), amorphous layer thickness (l_a), and transition layer thickness (E) are presented in Table III. It can be seen that the long period, which is the sum of the average thicknesses of the crystalline lamella and the amorphous region (l_c and l_a) is not drastically alternated with the SWCNTs loading. At low SWCNTs loading (0.05–0.1 wt %), in comparison to the neat PTT-PTMO copolymer the slightly decrease of long period for nanocomposites was observed. This can indicate that at low loading might form a larger number of smaller crystallites. Besides, the lamellar thickness growth is suppressed in nanocomposites especially at low loading of CNTs and can be attributed to the external confinement on nanometer scale introduced by the walls of the CNTs controlling the lamellar growth. At higher SWCNTs loading, the increase of long period was found mainly due to the increase of the amorphous layer thickness. The increase of amorphous layer thickness can be caused by the restriction of mobility of polymer chains caused by the existence of SWCNTs induced interfacial interactions between polymer and nanotubes.[57] The reduction of transition region thickness (E) was observed for all nanocomposites in comparison with neat PTT-PTMO copolymer. It can be a result of the increase of polarity of the crystalline phase due to the presence of CNTs.

Tensile properties

Representative stress–strain curves of the neat PTT-PTMO and nanocomposites measured at room temperature are presented in Figure 8. The corresponding characteristic values of these tests are presented in Table III. The yield stress and elongation of the nanocomposites is slightly influenced by the addition of the CNTs. The increase of Young's modulus is observed for composites at higher loading (0.2–0.5 wt %) of SWCNTs. The improvement in tensile strength are observed for nanocomposites at loading of SWCNTs from 0.05 to 0.3 wt %, while elongation at break remains unaffected or increases slightly on SWCNTs addition. In general, the tensile strength and modulus of semicrystalline polymer increase with the degree of crystallinity. However, here the degrees of crystallinity of PTT hard phase do not increase very significant (1.5–3%, Table IV) as the CNTs are loaded. It seems that improvement in tensile strength and modulus can be attributed not only to the change in crystallinity. The increase of tensile stress at break of nanocomposites can be a result of strong interfacial bonding between the (COOH) functionalized SWCNTs and PTT-PTMO matrix which can lead to the enhanced interfacial adhesion between them as well as uniform dispersion of the CNTs in PTT-PTMO matrix, thereby resulting in the improvement in the mechanical properties of the PTT-PTMO block copolymer nanocomposites at low loading of CNTs. However, at higher SWCNTs content, the improvement in the mechanical properties of PTT-PTMO block copolymer nanocomposites was not increased as expected. This behavior can be explained by the characteristics of SWCNTs, which have a tendency to bundle together in ropes due to van der Waals interaction. This tendency with combination of their high aspect ratio and large surface area could lead to form some agglomeration [as can be seen on Fig. 2(f)], causing the stress concentration phenomenon and preventing efficient load transfer to the polymer matrix.[5,48] As will be noted in many reports, most of randomly oriented polymer/CNTs composites show only a moderate or no strength enhancement, especially for composites containing untreated CNTs, mainly attributed to poor load transfer between polymer matrix and CNTs. The

TABLE IV
The Tensile Properties of PTT-PTMO/SWCNTs Nanocomposites

Sample	E (MPa)	σ_b (MPa)	ε_b (%)	σ_y (MPa)	ε_y (%)
PEE/0	67.8 ± 1.5	20.1 ± 1.9	755 ± 27	8.4 ± 0.1	47 ± 2
PEE/0.05	66.1 ± 1.1	26.0 ± 2.3	753 ± 30	8.6 ± 0.2	53 ± 1
PEE/0.1	67.7 ± 2.1	27.4 ± 2.9	750 ± 30	8.7 ± 0.2	53 ± 2
PEE/0.2	72.2 ± 2.3	23.0 ± 1.2	762 ± 26	8.7 ± 0.1	55 ± 3
PEE/0.3	72.8 ± 1.7	21.1 ± 1.1	772 ± 34	8.8 ± 0.1	57 ± 2
PEE/0.5	73.4 ± 2.2	18.9 ± 0.6	760 ± 26	9.0 ± 0.2	57 ± 2

E, Young's modulus; σ_b, stress at break; ε_b, strain at break; σ_y, ε_y, stress and strain at yield, respectively.

results obtained here are in contrast to the results obtained for PBT-PTMO/SWCNTs nanocomposites, where the Young's modulus and the yield strength were higher than those of neat PBT-PTMO block copolymer, but the elongation to break was less than a half.[7] Monitoring the changes in structure and morphology of the SWCNTs-filled and unfilled PBT-PTMO block copolymer studied as a function of deformation have shown that destruction is more efficient in the nanocomposite than in the copolymer, because stress is more efficiently transferred through the nanotubes anchored to the semicrystalline PBT blocks.[7]

CONCLUSIONS

Nanocomposites constituted by a poly(trimethylene terephthalate)-*block*-poly(tetramethylene oxide) (PTT-PTMO)-segmented copolymer and COOH-functionalized SWCNTs were prepared by *in situ* polymerization method. Microscopic analysis shows that the nanotubes are uniformly dispersed in the polymer matrix. However, at the highest loading (0.5 wt %) of CNTs in polymer matrix, the presence of small agglomerates of nanotubes was observed. As the SWCNs loading in the nanocomposites increase, the improvement of thermo-oxidative stability was observed. The morphology of PTT-PTMO copolymer consists of semicrystalline PTT domains dispersed in the soft matrix of amorphous, noncrystallizable PTMO. The glass transition temperature of PTMO-rich phase and melting temperature of semicrystalline PTT hard phase in nanocomposites were not influenced by presence of CNTs. CNTs were found to act as nucleating agents in nanocomposites. Thus, the presence of CNTs in PTMO-PTMO matrix increased the rate of the PTT hard phase crystallization (significant decrease of supercooling) due to heterogeneous nucleation. As the SWCNTs content increase, the degree of crystallinity of PTT hard phase in nanocomposites slightly increased. It was found that the long period slightly decrease at low CNTs loading (0.05–0.2 wt %). Enhancement of tensile strength of nanocomposites at low loading (0.05–0.3 wt %) of CNTs was observed. The results obtained have confirmed earlier results for semicrystalline nanocomposites that introduction of small quantity of CNTs uniformly dispersed in the polymer matrix will not increase drastically the macroscopic properties of semicrystalline polymers, unless a synergy is created between the CNTs and the crystalline lamellae of the polymer.

The authors thank for the financial support from the Polish National Science Centre in the fame of a grant no 2183/B/T02/2011/40.

References

1. Bhattacharya, S. N.; Kamal, M. R.; Gupta, R. K. Polymeric Nanocomposites: Theory and Practice; Carl Hanser Verlag: Munich, 2008; Chapter 2, p 5.
2. Paul, D. R.; Robeson, L. M. Polymer 2008, 49, 3187.
3. Moniruzzaman, M.; Winey, K. I. Macromolecules 2006, 39, 5194.
4. Coleman, J. N.; Khan, U.; Gun'ko, Y. K. Adv Mater 2006, 18, 689.
5. O'Connell, M. J. Carbon Nanotubes Properties and Applications; CRC Press Taylor & Francis Group: Boca Raton 2006; Chapter 8.
6. Gojny, F. H.; Wechmann, M. H. G.; Köpke, U.; Fiedler, B.; Schulze, K. Comp Sci Technol 2004, 64, 2363.
7. Hernández, J. J.; García-Gutiérrez, M. C.; Nogales, A.; Rueda, D. R.; Sanz, A.; Sics, I.; Hsiao, B. H.; Roslaniec, Z.; Broza, G.; Ezquerra, T. A. Polymer 2007, 48, 3286.
8. Hernández, J. J.; García-Gutiérrez, M. C.; Nogales, A.; Rueda, D. R.; Kwiatkowska, M.; Szymczyk, A.; Roslaniec, Z.; Concheso, A.; Guinea, I.; Ezquerra, T. A. Comp Sci Technol 2009, 69, 1867.
9. Gómez del Río, T.; Poza, P.; Rodríguez, J.; García-Gutiérrez, M. C.; Hernández, J. J.; Ezquerra, T. A. Comp Sci Technol 2010, 70, 284.
10. Szymczyk, A.; Roslaniec, Z.; Zenker, M.; García-Gutiérrez, M. C.; Hernández, J. J.; Rueda, D. R.; Nogales, A.; Ezquerra, T. A. Express Polym Lett 2011, 5, 977.
11. Nogales, A.; Broza, G.; Roslaniec, Z.; Schulte, K.; Sics, I.; Hsiao, B. S.; Santz, A.; García-Gutiérrez, M. C.; Rueda, D. R.; Domingo, C.; Ezquerra, T. A. Macromolecules 2004, 37, 7669.
12. García-Gutiérrez, M. C.; Nogales, A.; Rueda, D. R.; Domingo, C.; Gracía-Ramos, J. V.; Broza, G.; Roslaniec, Z.; Schulte, K.; Ezquerra, T. A. Comp Sci Technol 2007, 67, 798.
13. Fakirov, S. Handbook of Condensation Thermoplastic Elastomers; Wiley-VCH: Weinheim: 2005; Chapter 3.
14. Cella, R. J. J Polym Sci: Polym Symp 1973, 42, 727.
15. Szymczyk, A.; Nastalczyk, J.; Sablong, R. J.; Roslaniec, Z. Polym Adv Technol 2011, 22, 72.
16. Szymczyk, A.; Senderek, E.; Nastalczyk, J.; Roslaniec, Z. Eur Polym J 2008, 44, 436.
17. Bockstaller, M. R.; Mickiewicz, R. A.; Thomas, E. L. Adv Mater 2005, 17, 1331.
18. Szymczyk, A.; Roslaniec, Z. Polimery (Warsaw, in English) 2012, 57, 57.
19. Ma, Q.; Cebe, P. J Therm Anal Calorim 2010, 102, 42.
20. Wu, D.; Yang, T.; Sun, Y.; Shi, T.; Zhou, W.; Zhang, M. Polym Int 2011, 60, 1497.
21. Xu, Y. Jia, H. B.; Piao, J. N.; Ye, S. R.; Huang, J. J Mater Sci 2008, 43, 417.
22. Chuah, H. H. In: Modern Polyester: Chemistry and Technology of Polyesters and Copolyesters; Scheirs, J.; Long, T. E., Eds.; Wiley: Chichester, 2004; Chapter 11, p 361.
23. Rabiej, M.; Rabiej, S. WAXSFIT: A Computer Program for Analyzing X-Ray Diffraction Curves of Semicrystalline Polymers. ATH Scientific Publisher: Bielsko-Biała, 2006, 1.
24. Strobl, G. R.; Schneider, M. J Polym Sci Polym Phys Ed 1980, 18, 1343.
25. Strobl, G. R.; Schneider, M. J.; Voight-Martin, I. G. J Polym Sci Part A: Polym Chem 1980, 18, 1361.
26. Janicki, J. J Alloys Compd 2004, 382, 61.
27. Hsiao, B. S.; Verma, R. K. J Synchr Rad 1998, 5, 23.
28. Rabiej, S.; Rabiej, M. ATH Bielsko-Biała (in polish) 2009, 13.
29. Lee, J. K.; Im, J. E.; Lee, K. H. Macromol Res 2004, 12, 172.
30. Kwiatkowska, M.; Broza, G.; Schulte, K.; Roslaniec, Z. Rev Adv Mater Sci 2006, 12, 154.
31. Hernandez, Y.; Nicolosi, V.; Lotya, M.; Blighe, F. M.; Sun, Z.; De, S.; McGovern, I. T.; Holland, B.; Byrne, M.; Gun'Ko, Y. K.;

Boland, J. J.; Niraj, P.; Duesberg, G.; Krishnamurthy, S.; Goodhue, R.; Hutchison, J.; Scardaci, V.; Ferrari, A. C.; Coleman, J. N. Nat Nanotechnol 2008, 3, 563.
32. Hasan, T.; Scardaci, V.; Tan, P. H.; Rozhin, A. G.; Milne, W. I.; Ferrari, A. C. J Phys Chem C 2007, 111, 12594.
33. Tasis, D.; Tagmatarchis, N.; Bianco, A.; Prato, M. Chem Rev 2006, 106, 1105.
34. Kim, J. Y.; Han, S. I.; Hong, S. Polymer 2008, 49, 3335.
35. Kim, J. Y.; Han, S. I.; Kim, D. K.; Kim, S. H. Compos A 2009, 40, 45.
36. Spiros, T.; Drakonakis, V.; Mouzakis, D. E.; Fischer, D.; Gregoriou, V. G. Macromolecules 2006, 39, 9150.
37. Song, W.; Zheng, Z.; Tang, W.; Wang, X. Polymer 2007, 48, 3658.
38. Zhu, J.; Kim, J.; Peng, H.; Margrave, J. L.; Khabashesku, V. N.; Barrera, E. V. Nano Lett 2003, 3, 1107.
39. Szymczyk, A.; Rosłaniec, Z. Polimery (Warsaw) 2006, 51, 627.
40. Bothelho, G.; Gijsman, P.; Queiros, A. Polym Degr Stab 2001, 73, 431.
41. Zeynalov, E. B.; Friedrich, J. F. Open Mater Sci J 2008, 2, 28.
42. Watts, P. C. P.; Fearon, P. K.; Hsu, W. K.; Billingham, N. C.; Kroto, H. W.; Walton, D. R. M. J Mater Chem 2003, 13, 491.
43. Lu, K.; Grossiord, N.; Koning, C. E.; Miltner, H. E.; Van Mele, B.; Loos, J. Macromolecules 2008, 41, 8081.
44. Mitchell, C. A.; Krishnamoorti, R. Polymer 2005, 46, 8796.
45. Xu, Y.; Jia, H.-B.; Piao, J.-N.; Ye, S.-R.; Huang, J. J Mater Sci 2008, 43, 417.
46. Kodije, S. L.; Li, L.; Li, B.; Cai, C. Y.; Keating, M. J. Macromol Sci Part B 2006, 45, 231.
47. Brosse, A. C.; Tence'-Girault, S.; Piccione, P. M.; Leibler, L. Polymer 2008, 49, 4680.
48. García-Gutiérrez, M. C.; Hernández, J. J.; Nogales, A.; Panine, P.; Rueda, D. R.; Ezquerra, T. A. Macromolecules 2008, 41, 844.
49. Jin, J.; Song, M.; Pan, F. Thermochim Acta 2007, 456, 25.
50. Chatterjee, T.; Yurekli, K.; Hadjiev, V. G.; Krishnamoorti, R. Adv Funct Mater 2005, 15, 1832.
51. Müller, A. J.; Arnal, M. L.; Trujillo, M.; Lorenzo, A. T. Eur Polym J 2011, 47, 614.
52. Zhang, Z. W.; Xu, Q.; Chen, Z. M.; Yue, J. Macromolecules 2008, 41, 2868.
53. Li, L.; Li, B.; Hood, M. A.; Li, C. Y. Polymer 2009, 50, 953.
54. Yang, J.; Sidoti, G.; Liu, J.; Geil, P. H.; Li, C. Y.; Cheng, S. Z. D. Polymer 2001, 42, 7181l.
55. Ho, R. M.; Ke, K.-Z.; Chen, M. Macromolecules 2000, 39, 7529.
56. Desbourgh, I. J.; Hall, I. H.; Neisser, J. Z. Polymer 1979, 20, 545.
57. Bokoboza, L. Polymer 2007, 48, 4907.